Induced electrostatic fields in dense plasmas with an intense ultrashort pulse laser

S. Kato, A. Nishiguchi, and K. Mima
Institute of Laser Engineering, Osaka University, 2-6 Yamada-oka, Suita, Osaka, 565, Japan
(Received 7 February 1994)

The electrostatic fields induced by an intense laser field around an ion in a solid density plasma are investigated. In a plasma produced by irradiating an intense ultrashort pulse laser on a solid target, the electron and ion temperatures are not in thermal equilibrium, and the electron temperature is higher than the ion temperature. For such a plasma, the dynamical form factor of a plasma electron is derived. By using the dynamical form factor, the screened potential and the induced oscillating electrostatic field around an ion are obtained. As a result, the plasma screening effects on the direct ionization by the laser are clarified.

PACS number(s): 52.25.Rv, 52.40.Nk

I. INTRODUCTION

Recently, dense plasmas produced by an intense ultrashort pulse (pulse width less than 1 ps) laser have attracted much interest. In particular, the nonlinear plasma dynamics in the intense laser fields have become an interesting area [1]. An ultrashort pulse laser can heat a solid surface before the surface plasma expands. In such a case, the plasma density scale length is less than the laser skin depth. Consequently, the ultrashort pulse laser directly interacts with the solid density plasma. So far the plasma screening effects on the direct ionization of ions in the solid density plasma have not been investigated, although the effects have been discussed on the inverse bremsstrahlung absorption [2]. Moreover, when the electron temperature is lower than or comparable to the Fermi temperature, the ion-ion correlation and the electron screening are, in particular, important. The screened ion potential and electric field are evaluated by using the hypernetted-chain equation and the Lindhard linear response theory.

For dense plasmas, nonlinear inverse bremsstrahlung of high intensity laser is discussed by a previous paper [2]. The paper shows that the inverse bremsstrahlung absorption rate increases and then decreases with laser intensity, which depends on the ratios among ε_f, $mv_0^2/2$, and T_e, where v_0, ε_f, and T_e are the electron quiver velocity, the Fermi energy, and the electron temperature, respectively. Note that the inverse bremsstrahlung absorption includes only free-free transitions. However, the laser absorption by the above-threshold-ionization (ATI) or tunneling ionization (TI) that is a bound-free transition is more important than the inverse bremsstrahlung absorption when the laser pulse width is comparable to ionization time.

The ionization processes by the intense short pulse laser have been investigated by the theory and/or simulation [3–8]. Since the perturbation methods are not applicable to investigate the effects of the intense external electric field, a new approximation and a new analytical method to describe the TI are developed by several authors [3,4]. Keldysh derived a formula for the ionization rate of TI by evaluating the transition probability between the Volkov states and the unperturbed bound states [3]. Recently, the Schrödinger equation for an electron atom in the strong laser field was numerically solved by using the super computer. The many interesting behaviors of an electron which feels both atomic potential and the external electric field are discovered [1,5–8]. The experiments of the TI for noble gases are analyzed by the Keldysh model and other theories [9–11]. The collisional ionization rates are also investigated for electron distribution functions which are deformed by intense laser fields [12–14].

When the intense ultrashort pulse irradiates a solid target, the laser field penetrates into a solid density plasma when plasma density scales; L_d length is very short, namely, $L_d \ll c/\omega_0$, where c and ω_0, are the speed of light and the laser frequency, respectively. For the ATI or TI in a solid density plasma, a bound electron in an atom can be excited and/or ionized by not only the external laser field but also the induced field of the dense plasma. So far the induced electrostatic fields in the solid density plasmas with the laser field have not been treated. Therefore this paper discusses the induced field in relation with the plasma polarization. The screened ion potential and electric field are derived by using the linear response theory in Sec. II. In Sec. III, the screening ion potentials and laser fields are calculated by using the hypernetted-chain equation and the dielectric response function. Some concluding remarks are given in Sec. IV.

II. DERIVATION OF INDUCED FIELDS

The screened electrostatic potential and the electric field which acts on the bound electron are derived in the frame which oscillates with an electron excursion length $\mathbf{r}_0(t)$ We assumed that the laser light is linearly polarized and the laser intensity is constant, namely, $\mathbf{E}_L(t)=\mathbf{E}_0\sin\omega_0 t$. Then $\mathbf{r}_0(t)=\mathbf{r}_0\sin\omega_0 t$, and $\mathbf{r}_0=-e\mathbf{E}_0/m\omega_0^2$. This oscillation frame was introduced by analyzing the inverse bremsstrahlung in the plasmas [2,15,16]. In the analysis of the ionization called by the intense laser fields, the above oscillating is called the Kramers-

Henneberger (KH) frame [17].

The electric fields around an ion in the dense plasma are determined as follows:

$$\mathbf{E}(\mathbf{r},t)=\mathbf{E}_L(t)=\nabla\Phi_{os}(\mathbf{r}-\mathbf{r}_0(t),t) , \tag{1}$$

where $\Phi_{os}(\mathbf{r},t)$ is the electrostatic potential obtained in the oscillation (KH) frame and the ion is put at the origin of the coordinate in the laboratory frame. In the following analysis, the effects of bound electron polarization on the generation of the induced electric field is neglected, because the number of free electrons contributing to generating the induced field is much greater than the number of bound electron.

In the oscillation frame, $\Phi_{os}(\mathbf{r},t)$ satisfied

$$-\nabla^2\Phi_{os}(\mathbf{r},t)=4\pi e[Z^*\delta(\mathbf{r}+\mathbf{r}_0(t)) +Z^*n_i g_i(\mathbf{r}+\mathbf{r}_0(t))-n_e(\mathbf{r},t)] , \tag{2}$$

where n_i and Z^*e are the ion number density and effective ion charge. $g_i(\mathbf{r})$ is the radial distribution function of ions plasma around a test ion, which is assumed to be fixed. $n_e(\mathbf{r},t)$ is electron number density. The background plasma is assumed to be neutral: $Z^*n_i=n_e$. Then, we obtain

$$-\nabla^2\Phi_{os}(\mathbf{r},t)=4\pi e[Z^*\delta(\mathbf{r}+\mathbf{r}_0(t)) +Z^*n_i h(\mathbf{r}+\mathbf{r}_0(t))-\delta n_e(\mathbf{r},t)] , \tag{3}$$

where

$$h(\mathbf{r}+\mathbf{r}_0(t))=g(\mathbf{r}+\mathbf{r}_0(t))-1 , \tag{4}$$

$$\delta n_e(\mathbf{r},t)=n_e(\mathbf{r},t)-n_e , \tag{5}$$

and $\delta n_e(\mathbf{r},t)$ and $h(\mathbf{r})$ are the electron density fluctuation and pair correlation function. The Fourier transform of Eq. (3) yields

$$\Phi_{os}(\mathbf{k},\omega)=-\frac{4\pi e}{k^2}\left[Z^*S(\mathbf{k})\sum_{n=-\infty}^{\infty}J_n(\mathbf{k}\cdot\mathbf{r}_0)2\pi\delta(\omega+n\omega_0)-\delta n_e(\mathbf{k},\omega)\right] , \tag{6}$$

and the ion form factor $S(\mathbf{k})$ is given by

$$S(\mathbf{k})=1+n_i\int d\mathbf{r}\,h(\mathbf{r})\exp(-i\mathbf{k}\cdot\mathbf{r}) , \tag{7}$$

where ω_0 is the laser frequency. Using the linear response theory, $\delta n_e(\mathbf{k},\omega)$ is given by

$$\delta n_e(\mathbf{k},\omega)=[\varepsilon(\mathbf{k},\omega)-1]\frac{k^2\Phi_{os}(\mathbf{k},\omega)}{4\pi e} , \tag{8}$$

where $\varepsilon(\mathbf{k},\omega)$ is the dielectric response function. From Eqs. (6) and (8), the screened ion potential $\Phi_{os}(\mathbf{k},\omega)$ is obtained as follows:

$$\Phi_{os}(\mathbf{k},\omega)=-\frac{4\pi Z^*e}{k^2}\frac{S(\mathbf{k})}{\varepsilon(\mathbf{k},\omega)} \times\sum_{n=-\infty}^{\infty}J_n(\mathbf{k}\cdot\mathbf{r}_0)2\pi\delta(\omega+n\omega_0) . \tag{9}$$

The inverse Fourier transform of Eq. (9) yields

$$\Phi_{os}(\mathbf{r},t)=\sum_{n=-\infty}^{\infty}\phi_n(\mathbf{r},t)\exp(in\omega_0 t) , \tag{10}$$

where

$$\phi_n(\mathbf{r},t)=-\int\frac{d\mathbf{k}}{(2\pi)^3}\frac{4\pi Z^*e}{k^2}\frac{S(\mathbf{k})}{\varepsilon(\mathbf{k},-n\omega_0)} \times J_n(\mathbf{k}\cdot\mathbf{r}_0)\exp(i\mathbf{k}\cdot\mathbf{r}) . \tag{11}$$

Setting $S(\mathbf{k})=1$ and $\varepsilon(\mathbf{k},\omega)=1$, Eqs. (9) and (10) are reduced to the pure Coulomb potential in the oscillating frame,

$$\Phi_C(\mathbf{r},t)=-\frac{Z^*e}{|\mathbf{r}+\mathbf{r}_0(t)|} =-\sum_{n=-\infty}^{\infty}\int\frac{d\mathbf{k}}{(2\pi)^3}\frac{4\pi Z^*e}{k^2} \times J_n(\mathbf{k}\cdot\mathbf{r}_0)\exp[i(\mathbf{k}\cdot\mathbf{r}+n\omega_0 t)] . \tag{12}$$

Using Eq. (12), we separate the pure Coulomb potential from $\Phi_{os}(\mathbf{r},t)$ as follows:

$$\Phi_{os}(\mathbf{r},t)=\Phi_C(\mathbf{r},t)+\Phi_P(\mathbf{r},t) , \tag{13}$$

where $\Phi_P(\mathbf{r},t)$ represents the plasma screening effects. The plasma screening effects are then given as follows:

$$\Phi_P(\mathbf{r},t)=\sum_{n=-\infty}^{\infty}\phi_{Pn}(\mathbf{r},t)\exp(in\omega_0 t) , \tag{14}$$

where

$$\phi_{Pn}(\mathbf{r},t)=-\int\frac{d\mathbf{k}}{(2\pi)^3}\frac{4\pi Z^*e}{k^2}\left[\frac{S(\mathbf{k})}{\varepsilon(\mathbf{k},-n\omega_0)}-1\right] \times J_n(\mathbf{k}\cdot\mathbf{r}_0)\exp(i\mathbf{k}\cdot\mathbf{r}) . \tag{15}$$

The electrostatic potential in the laboratory frame is then obtained from Eq. (12) as

$$\Phi(\mathbf{r},t)=\Phi_{os}(\mathbf{r}-\mathbf{r}_0(t),t) =-\frac{Z^*e}{|r|}+\sum_{n=-\infty}^{\infty}\phi_{Pn}(\mathbf{r}-\mathbf{r}_0(t),t)\exp(in\omega_0 t) , \tag{16a}$$

or

$$\Phi(\mathbf{r},t)=-\frac{Z^*e}{|\mathbf{r}|}+\sum_{n=-\infty}^{\infty}\phi_{\text{lab }Pn}(\mathbf{r})\exp(in\omega_0 t) , \tag{16b}$$

where

$$\phi_{Pn}(\mathbf{r}-\mathbf{r}_0(t),t)=-\int\frac{d\mathbf{k}}{(2\pi)^3}\frac{4\pi Z^*e}{k^2}\left[\frac{S(\mathbf{k})}{\varepsilon(\mathbf{k},-n\omega_0)}-1\right]J_n(\mathbf{k}\cdot\mathbf{r}_0)\exp\{i\mathbf{k}\cdot[\mathbf{r}-\mathbf{r}_0(t)]\}\ . \tag{17}$$

Thus the higher harmonic components of the induced electric field in the laboratory frame $\phi_{\text{lab }Pn}(\mathbf{r})$ is obtained by expanding $\exp\{i\mathbf{k}\cdot[\mathbf{r}-\mathbf{r}_0(t)]\}$ of Eq. (17) into a Fourier series as follows:

$$\phi_{\text{lab }Pn}(\mathbf{r})=-\sum_{m=-\infty}^{\infty}\int\frac{d\mathbf{k}}{(2\pi)^3}\frac{4\pi Z^*e}{k^2}\left[\frac{S(\mathbf{k})}{\varepsilon(\mathbf{k},-m\omega_0)}-1\right]J_m(\mathbf{k}\cdot\mathbf{r}_0)J_{m-n}(\mathbf{k}\cdot\mathbf{r}_0)\exp(i\mathbf{k}\cdot\mathbf{r})\ . \tag{18}$$

Note that $\phi_{\text{lab }P(n=0)}$ represents the static screened potential which is relevant to the ionization potential lowering effects. In the high density and degenerate plasmas, the effects of the screening static potential on the atomic levels are important and been widely investigated by many authors [18–21]. In the following discussion, the effects of the ionization potential lowering on the ATI and/or TI are discussed.

In the laboratory frame, the total electric field is represented as

$$\mathbf{E}(\mathbf{r},t)=\mathbf{E}_L(t)+\mathbf{E}_{\text{ind}}(\mathbf{r},t)=\mathbf{E}_L(t)-\nabla\Phi(\mathbf{r},t)\ , \tag{19}$$

where $\mathbf{E}_L(t)=\mathbf{E}_0\sin\omega_0 t$,

$$\mathbf{E}_{\text{ind}}(\mathbf{r},t)=\sum_{n,m=-\infty}^{\infty}\int\frac{d\mathbf{k}}{(2\pi)^3}\frac{4\pi Z^*e}{k^2}\left[\frac{S(\mathbf{k})}{\varepsilon(\mathbf{k},-m\omega_0)}-1\right]J_m(\mathbf{k}\cdot\mathbf{r}_0)J_{m-n}(\mathbf{k}\cdot\mathbf{r}_0)i\mathbf{k}\exp[i(\mathbf{k}\cdot\mathbf{r}+n\omega_0 t)]\ . \tag{20}$$

In the limit of small electron excursion length, the lowest order laser induced field is proportional to the excursion length. It is clear from Eq. (20) that the lowest order field induced by laser come from $(m=\pm1,n=\pm1)$ and $(m=0,n=\pm1)$. Note that the terms for $n=0$ vanish in Eq. (20), since the integrand of Eq. (20) of $\mathbf{k}$ because of $J_m^2(\mathbf{k}\cdot\mathbf{r})$ is the even function of $\mathbf{k}\cdot\mathbf{r}$ and $S(\mathbf{k})$ and $\varepsilon(\mathbf{k})$ are the even functions of $\mathbf{k}$.

III. NUMERICAL CALCULATIONS OF INDUCED ELECTRIC FIELD

The electric field at the origin (at the ion nucleus) $\mathbf{E}(\mathbf{r}=\mathbf{0},t)$ is numerically calculated in this section, since it will be enough for estimating the induced field effects on ATI and/or TI. We represent $\mathbf{E}_{\text{ind}}(\mathbf{r}=0,t)$ as follows:

$$\mathbf{E}_{\text{ind}}(\mathbf{r}=0,t)=\sum_{n=-\infty}^{\infty}\mathbf{E}_n\exp(in\omega_0 t)\ , \tag{21}$$

where

$$\mathbf{E}_n=\sum_{m=-\infty}^{\infty}\int\frac{d\mathbf{k}}{(2\pi)^3}\frac{4\pi Z^*e}{k^2}\left[\frac{S(\mathbf{k})}{\varepsilon(\mathbf{k},-m\omega_0)}-1\right]\times J_m(\mathbf{k}\cdot\mathbf{r}_0)J_{m-n}(\mathbf{k}\cdot\mathbf{r}_0)i\mathbf{k}\ . \tag{22}$$

If the dielectric response function does not depend on the frequency, namely, $\varepsilon(\mathbf{k},\omega)\approx\varepsilon(\mathbf{k},0)$, the induced fields vanish since the integral of Eq. (22) over $\mathbf{k}$ vanishes. Therefore the electron dynamics is essential for the generation of the induced electric field. We assumed that the dielectric response function and the ion structure factor are isotropic, namely, $\varepsilon(\mathbf{k},\omega)=\varepsilon(k,\omega)$, $S(\mathbf{k})=S(k)$. Then, the electrostatic field of Eq. (22) is given by

$$\mathbf{E}_{nz}=\sum_{m=-\infty}^{\infty}\frac{4\pi Z^*e}{(2\pi)^2}2i\delta_{n\,\text{odd}}\times\int_0^\infty k\,dk\left[\frac{S(k)}{\varepsilon(k,-m\omega_0)}-1\right]\times\int_0^1 x\,dx\,J_m(kr_0x)J_{m-n}(kr_0x)\ , \tag{23}$$

where $\delta_{n\,\text{odd}}=1$, when $n=$odd, otherwise, 0. In Eq. (23), the laser polarization direction is assumed along a z axis. Furthermore, Eq. (23) indicates that the induced field has only odd harmonics. The summation in Eq. (22) is taken up to $|m|=80$ in the numerical calculation.

Let us discuss here the validity of the linear response approximation for the electron dynamics, when the electron-ion and electron-electron couplings are weak, the electron response is described by the linear dielectric constant $\varepsilon(\mathbf{k},\omega)$. The dielectric response function included the electron degeneracy effect which is called the Lindhard dielectric function. Of course, it may be possible to use $\varepsilon(\mathbf{k},\omega)$ which includes the local field correction given by Ichimaru *et al.* [18]. The local field correction is important, when the electron temperature is very low and the electron density is not high enough.

The dielectric response function of the partially degenerate collisionless plasmas have been given in a previous paper [2,22]. In the plasma produced by the ultrashort pulse laser, the ion is usually strongly coupled, namely $10\geq\Gamma_i\geq1$, where Γ_i is the Coulomb coupling constant and defined by

$$\Gamma_i=\frac{Z^{*2}e^2}{a_iT_i}\ ,$$

where a_i is the average ion radius $(3/4\pi n_i)^{\frac{1}{3}}$. For the medium ion correlation $1\leq\Gamma_i\leq10$ the ion structure factor is known to be well approximated by the

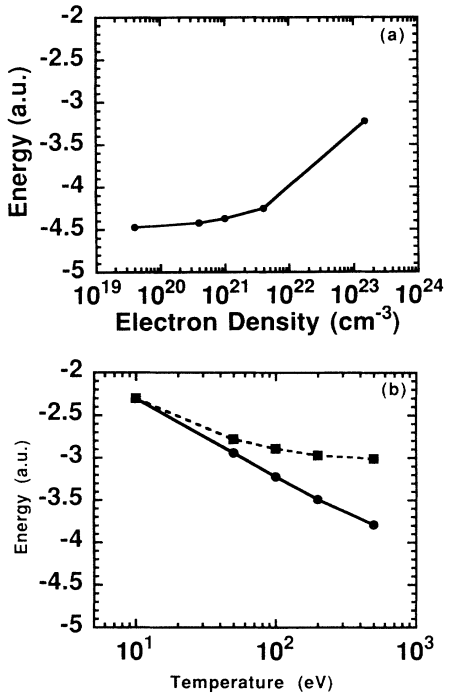

FIG. 1. Energy level of the grand state for the lithium plasmas. Figure (a) shows the electron density dependence for $T_e = T_i = 100$ eV. Figure (b) shows the electron temperature dependence for the solid density. The solid and dotted lines show $T_e = T_i$ and $T_i = 10$ eV.

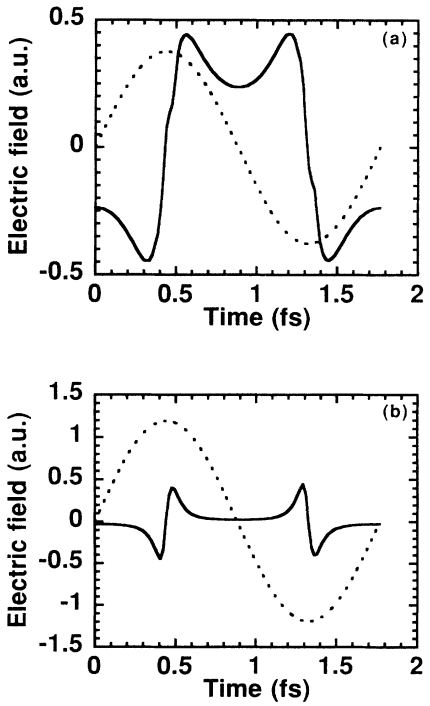

FIG. 2. Time evolution of the laser and induced field for $T_e = 100$ eV, $T_i = T_e$, $n_e = 1.5 \times 10^{23}$ cm^{-3}, $n_i = 5.0 \times 10^{22}$ cm^{-3}, $Z^* = 3$. The solid and broken lines show the induced and laser field, respectively. Figures (a) and (b) are for laser intensity; $I_L = 10^{16}$ and 10^{17} W/cm^2, respectively.

hypernetted-chain equation model [23,24]. The detailed formulae of the electron dielectric response function and the ion static form factor were described in a previous paper [2].

When there is no laser field, the energy levels of the bound state in the present plasma model are shown in Figs. 1(a) and 1(b). The ionization potential lowerings are estimated by the electrostatic potential Eq. (18) at $r_0 = 0$. We consider a lithium plasma ($Z = 3$), namely, the bound energy of grand state for a hydrogen like Li is -4.5 a.u. Figure 1(a) shows the electron density dependence of the bound energy for $T_e = T_i = 100$ eV. The energy lowering is less than the 10% for the density lower then the cutoff density of the laser wavelength 0.53 μm. Figure 1(b) shows the temperature dependence of the electron binding energy in the solid density plasmas. The binding energy decreases with decrease of the plasma temperature, because the screening distance becomes shorter when the

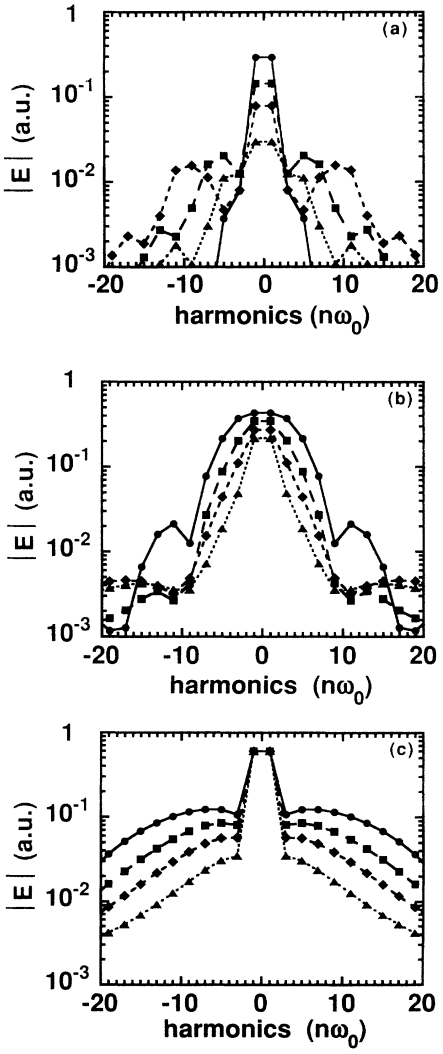

FIG. 3. Amplitudes of fundamental and harmonics for $T_i = T_e$, $n_e = 1.5 \times 10^{23}$ cm^{-3}, $n_i = 5.0 \times 10^{22}$ cm^{-3}, $Z^* = 3$. The circle, square, diamond, and triangle are for electron temperature; $T_e = 10$, 50, 100, and 200 eV, respectively. Figures (a), (b), and (c) are for laser intensity; $I_L = 10^{14}$, 10^{16}, and 10^{17} W/cm^2, respectively.

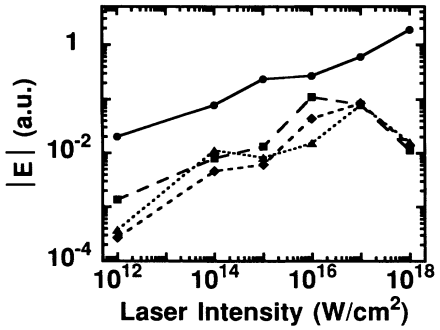

FIG. 4. Amplitudes of fundamental and harmonics as a function of laser intensity for $T_e=100$ eV, $T_i=T_e$, $n_e=1.5\times10^{23}$ cm^{-3}, $n_i=5.0\times10^{22}$ cm^{-3}, $Z^*=3$. The circle, square, diamond, and triangle show $n=1$, 3, 5, and 7.

temperature decreases. The ionization energy lowering enhances the ionization rate, as discussed in Sec. IV.

For example, the ion density is assumed to be the solid lithium, namely, $n_i=5\times10^{22}$ cm^{-3}, $Z^*=3$, $n_e=Z^*n_i=1.5\times10^{23}$ cm^{-3}. We also assume that the Fermi temperature is 10 eV, the laser wavelength is 0.53 μm, and the cutoff density $n_c=4\times10^{21}$ cm^{-3}. Then $n_e/n_c\approx37.5$ and $\omega_p/\omega_0\approx6.12$. Figures 2(a) and 2(b) show the temporal evolutions of the induced field given by Eq. (21) with Eq. (23) for the laser intensity $I_L=10^{16}$ and 10^{17} W/cm^2, respectively. The electric fields are normalized by the atomic units. The phase of the induced electric field shifts from that of the source laser field shifts by 20°–30°; this shift is proportional to the imaginary part of the electron dielectric response function. Namely, the laser absorption by the inverse bremsstrahlung is related to this phase shift. The deformation of the wave form of the induced fields from the sinusoidal wave in Fig. 2(b) indicates that higher harmonics are generated strongly. The bound electron in the ion is perturbed by both the laser fields and the induced fields. Since the induced fields are greater than or comparable to the input laser field in Fig. 2(a), the effects of the induced fields have to be taken into account in the analysis of the photoionization process in dense plasmas. The ionization rates influenced by the induced fields are discussed in Sec. IV.

The fundamental and higher harmonics obtained from Eq. (23) for various electron temperatures are shown in Figs. 3(a)–3(c), where the fundamental field includes the input laser field. Here, we assume that $T_i=T_e$, and the laser intensities are $I_L=10^{14}$, 10^{16}, and 10^{17} W/cm^2, for Figs. 3(a)–3(c), respectively. Figure 3 shows that the amplitudes of the lower order harmonics, namely, $n=3$ and 5, become maximum at the optimum laser intensities. The amplitudes of the fundamental and harmonics as functions of the laser intensity for $T_e=100$ eV are shown in Fig. 4, for $n=1$, 3, 5, and 7. The fundamental field is enhanced, where the laser intensity is less than 10^{16} W/cm^2. The $n=3$ harmonic amplitude becomes maximum at $I_L=10^{16}$ W/cm^2 for the present plasma parameters. The higher harmonics of $n\geq11$, increase when the laser intensities increase up to $I_L=10^{18}$ W/cm^2. In order to investigate the mechanisms of the existence of the optimum laser intensity, the plasma density dependence of

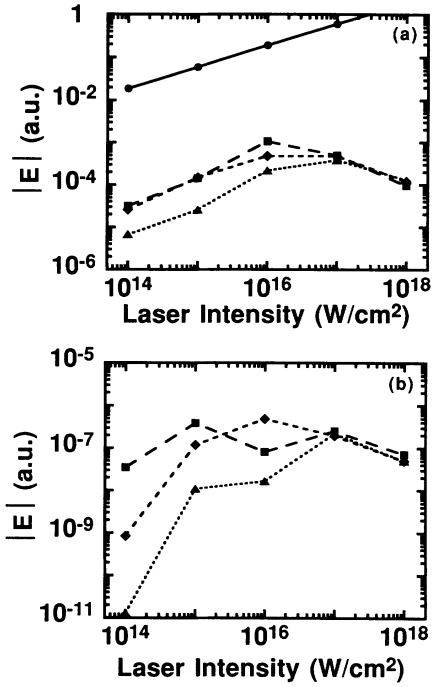

FIG. 5. Amplitudes of fundamental and harmonics as a function of laser intensity for $T_e=100$ eV, $T_i=T_e$, $n_i=n_e/Z^*$, $Z^*=3$. Figures (a) and (b) are for electron density; $n_e=4.0\times10^{21}$ and 4.0×10^{19} cm^{-3}, respectively. The circle, square, diamond, and triangle show $n=1$, 3, 5, and 7, respectively.

the harmonics is numerically calculated as shown in Figs. 5(a) and 5(b). For $n_e=n_c$ and $n_e=n_c/100$, the fundamental and harmonic amplitudes as a function of the laser intensity are shown in Figs. 5(a) and 5(b). The optimum laser intensity is lower, when the plasma density is lower. We interpret the above laser intensity dependences of the generation of the higher harmonics, as follows. Let us consider the ratios of the excursion length r_0 to the average ion radius a_i and Debye length λ_D and the ratios of the laser field E_L to the Coulomb field around ion Z^*e/a_i^2 and Z^*e/λ_D^2. For the laser wavelength 0.53 μm, those ratios are given as follows:

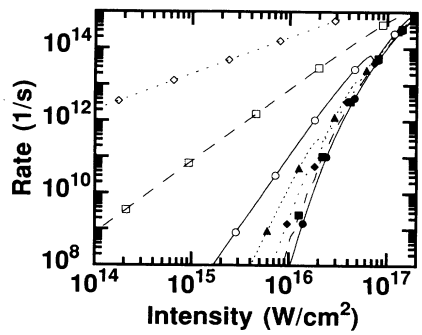

FIG. 6. Ionization rate as a function of laser intensity, where the ionization energy and the fundamental wavelength are 87 eV and 0.53 μm. The closed circle, square, diamond, and triangle show the fundamental 3rd, 5th, and 7th harmonics, respectively. The open circle, square, and diamond show 11th, 21st, and 41st harmonics, respectively.

$$L_1 \equiv r_0/a_i \cong 15 \left[\frac{[I_L\ (\mathrm{W/cm^2})]}{10^{16}}\right]^{1/2} \left[\frac{[n_i\ (\mathrm{cm^{-3}})]}{5\times 10^{22}}\right]^{1/3}$$

$$L_2 \equiv r_0/\lambda_D \cong 14 \left[\frac{[I_L\ (\mathrm{W/cm^2})]}{10^{16}}\right]^{1/2} \left[\frac{[n_i\ (\mathrm{cm^{-3}})]}{5\times 10^{22}}\right]^{1/2} \left[\frac{100}{[T\ (\mathrm{eV})]}\right]^{1/2},$$

$$E_1 \equiv \frac{E_L}{Z^* e/a_i^2} \cong 1.3 \left[\frac{3}{Z^*}\right] \left[\frac{[I_L\ (\mathrm{W/cm^2})]}{10^{16}}\right]^{1/2} \left[\frac{5\times 10^{22}}{[n_i\ (\mathrm{cm^{-3}})]}\right]^{1/2},$$

and

$$E_2 \equiv \frac{E_L}{Z^* e/\lambda_D^2} \cong 1.4 \left[\frac{3}{Z^*}\right]^2 \left[\frac{[I_L\ (\mathrm{W/cm^2})]}{10^{16}}\right]^{1/2} \left[\frac{5\times 10^{22}}{[n_i\ (\mathrm{cm^{-3}})]}\right] \left[\frac{100}{[T\ (\mathrm{eV})]}\right].$$

When the L_1 (for strong coupling) or L_2 (for weak coupling) is greater than unity, the electron motion becomes nonlinear and the higher harmonics are generated. On the other hand, the induced plasma fields, which may be limited by the Coulomb field around the ion are negligible in comparison with the laser field, when E_1 or E_2 is much greater than unity. Therefore the electron oscillation becomes sinusoidal and the harmonic generation will be ineffective. Therefore, the harmonic generation becomes maximum when E_1 or $E_2 \approx 1$ and L_1 or $L_2 > 1$.

IV. CONCLUDING REMARKS

We derive the screened ion potentials and the induced electrostatic fields in dense plasmas with intense laser fields. The screened ion potential and electric field are evaluated by using the hypernetted-chain equation and the linear response theory. For the solid density plasmas, the screened potential and energy level lowering are evaluated. In our evaluation, the free electron polarization is treated by the dielectric response function where the electron local-field correction is ignored although the ion-ion strong correlation is included. The ionization energy lowering or wave function modification due to the static plasma shielding is found to be important for the direct ionization rate. The enhancements of the ionization rate due to the ionization potential lowering are evaluated by using the Keldysh or Reiss formula [3,4]. Furthermore, in order to show that the induced oscillating electric field effects on the laser direct ionization, the induced electric fields are evaluated. The numerical calculations are carried out to obtain the oscillating electric fields at an ion nucleus. We find that the induced electrostatic fields are comparable to the external laser field, for dense plasmas. For the solid density plasmas, the atomic processes and harmonic emissions will be significantly modified by the plasma polarization.

It is discussed how the ionization rates are enhanced by the laser induced fields. The ionization rates are evaluated by the Keldysh formula. It is assumed that the wave function of the ground state is not distorted by the laser field and the hydrogenlike properties. This model is applicable and commonly used to evaluate the ionization by intense laser-atom interactions, when the photon energy is less than the ionization energy. It has been checked that the Keldysh theory agrees well with the experimental results for the low Z atoms [11]. Since the ionization rate is sensitive to the ionization energy, it is necessary to take into account the ionization energy lowering in the solid density plasmas. The radiation intensity dependences of ionization rate for various harmonics is shown in Fig. 6, where the ionization rates for the solid density lithium with the temperature of 100 eV. In this case, the ionization energy is 87 eV, the laser wavelength is 0.53 μm, and the photon energy is 2.2 eV. When the field intensity is 10^{16} W/cm^2, the ionization rate for the fundamental is less than 10^9 s^{-1}, while it is greater than 10^9 s^{-1} for the fifth harmonic and greater than 10^{12} s^{-1} for the 21th harmonic field. Note in Fig. 6 also that the ionization rate is greater than 10^9 s^{-1} for the 21st harmonic and greater than 10^{12} s^{-1} for the 41st harmonic, when the field intensity is 10^{14} W/cm^2. Moveover, the ionization rate for the fundamental is greater than 10^9 s^{-1}, when the field intensity is 1.4×10^{16} W/cm^2.

In the laser intensity region of a few 10^{16} W/cm^2, the ionization rates strongly depend on the photon energy and intensity. The enhancement of the fundamental field and generation of the harmonics up to the seventh are shown in Fig. 4, where the laser intensity is from 10^{12} W/cm^2 to 10^{18} W/cm^2. In this case, the ionization rate for $I_L = 10^{15}$ W/cm^2 and 10^{16} W/cm^2 is enhanced to be greater than 10^9 s^{-1}, because the fundamental fields for $I_L = 10^{15}$ W/cm^2 and 10^{16} W/cm^2 are greater than 1.4×10^{16} and 2×10^{16} W/cm^2. When the intensity is higher than 10^{17} W/cm^2, the ionization rates are dominated by the input laser fields, because of very efficient tunneling ionization. Note here that the Keldysh model is not applicable to the 41st harmonic field, because the photon energy is greater than the ionization energy.

The more precise ionization rate evaluation is required as for the effects of the multifrequency fields, because the Keldysh formula gives the precise ionization rate for the monochromatic laser field. Namely, the formula is not applicable to the multifrequency induced fields. Actually, in the case of the multifrequency fields, the ionization rate is predicted to be greater than the monochromatic field [25–27].

Although, the ionization processes in cold plasmas on solid targets are theoretically investigated by many authors [28–30], the multihigher harmonics effects have not

been investigated. In this case, not only the ionization energy lowering but also the multiharmonics generation will strongly affect the ionization processes. Namely, in order to evaluate the direct ionization rates in solid density plasmas, we have to solve the Schrödinger equation for bound electrons in an ion by taking into account the dynamical screening. The precise studies of the direct ionization by solving the appropriate Schrödinger equation will be presented in a following paper.

When the laser intensity $I\lambda^2$ is higher than 10^{18} W $\mu m^2/cm^2$, where the electron quiver velocity is comparable to the speed of light, namely, the relativistic effects are essential for the plasma dynamics, our present formula is no longer valid. For example, the magnetic field of the laser radiation will play very important roles in the photoionization process, which has been neglected in the analysis of this paper. The relativistic corrections on the direct ionization processes will be also discussed further in following works.

ACKNOWLEDGMENTS

We would like to thank Professor K. Nishihara, Professor H. Takabe at the Institute of Laser Engineering, Osaka University, and Dr. H. Furukawa at the Institute for Laser Technology for many useful discussions. This work was partially supported by the Grant-in-Aid for Scientific Research from the Ministry of Education, Science, and Culture of Japan and by the Japan Society for the Promotion of Science for Japanese Junior Scientists.

[1] F. Brunel, J. Opt. Soc. Am. B **7**, 521 (1990).
[2] S. Kato, R. Kawakami, and K. Mima, Phys. Rev. A **43**, 5560 (1991).
[3] L. V. Keldysh, Zh. Eksp. Teor. Fiz. **47**, 1945 (1964) [Sov. Phys. JETP **20**, 1307 (1965)].
[4] H. R. Reiss, Phys. Rev. A **22**, 1786 (1980).
[5] J. Opt. Soc. Am. B **7**, 403 (1990).
[6] Q. Su and J. H. Eberly, Phys. Rev. A **43**, 2474 (1991).
[7] M. Pont, N. R. Walet, and M. Gavrila, Phys. Rev. A **41**, 477 (1990).
[8] V. C. Reed and K. Burnett, Phys. Rev. A **46**, 424 (1992).
[9] M. D. Perry, A. Szoke, O. L. Landen, and E. M. Campbell, Phys. Rev. Lett. **60**, 1270 (1988).
[10] S. Augst, D. Strickland, D. D. Meyerhofer, S. L. Chin, and J. H. Eberly, Phys. Rev. Lett. **63**, 2212 (1989).
[11] G. Gibson, T. S. Luk, and C. K. Rhodes, Phys. Rev. A **41**, 5049 (1990).
[12] A. Brunce Langdon, Phys. Rev. Lett. **44**, 575 (1980).
[13] B. N. Chichkov, S. A. Shumsky, and S. A. Uryupin, Phys. Rev. A **45**, 7475 (1992).
[14] Boris N. Chichkov and Ernst E. Fill, Opt. Commun. **78**, 35 (1990).
[15] J. Dawson and C. Oberman, Phys. Fluids **5**, 517 (1962); J. Dawson, in *Advance in Plasma Physics,* edited by A. Simon and W. B. Thompson (Wiley, New York, 1969), Vol. 1, p. 1.
[16] R. D. Jones and K. Lee, Phys. Fluids **25**, 2307 (1982).
[17] W. C. Henneberger, Phys. Rev. Lett. **21**, 838 (1968).
[18] S. Ichimaru, S. Mitake, S. Tanaka, and X.-Z. Yan, Phys. Rev. A **32**, 1768 (1985).
[19] F. Perrot, Y. Furutani, and M. W. C. Dharma-wardana, Phys. Rev. A **41**, 1096 (1990).
[20] Xin-Zhong Yan, Shih-tung Tasi, and Setsuo Ichimaru, Phys. Rev. A **43**, 3057 (1991).
[21] H. Furukawa and K. Nishihara, Phys. Rev. A **46**, 6596 (1992).
[22] E. M. Lifshitz and L. P. Pitaevskii, *Physical Kinetics* (Pergamon, New York, 1981), Sec. 40.
[23] Kin-Chue Ng, J. Chem. Phys. **61**, 2680 (1974).
[24] R. Kawakami, K. Mima, H. Totsuji, Y. Yokoyama, Phys. Rev. A **38**, 3618 (1988).
[25] M. E. Goggin and P. W. Milonni, Phys. Rev. A **38**, 5174 (1988).
[26] C. M. Bowden, S. D. Pethel, and C. C. Sung, Phys. Rev. A **46**, 597 (1992).
[27] M. Protopapas, P. L. Knight, and K. Burnett, Phys. Rev. A **49**, 1945 (1994).
[28] N. H. Burnett and P. B. Corkum, J. Opt. Soc. Am. B **6**, 1195 (1989).
[29] B. M. Penetrante and J. N. Bardsley, Phys. Rev. A **43**, 3100 (1991).
[30] S. C. Rae and K. Burnett, Phys. Rev. A **46**, 2077 (1992).